Enhanced Ordering of Interacting Filaments by Molecular Motors

Pavel Kraikivski, Reinhard Lipowsky, and Jan Kierfeld
Max Planck Institute of Colloids and Interfaces, Science Park Golm, 14424 Potsdam, Germany
(Received 12 November 2005; published 29 June 2006)

We theoretically study the cooperative behavior of cytoskeletal filaments in motility assays in which immobilized motor proteins bind the filaments to substrate surfaces and actively pull them along these surfaces. Because of the mutual exclusion of the filaments, the coupled dynamics of filaments, motor heads, and motor tails leads to a nonequilibrium phase transition which generalizes the isotropic-nematic phase transition of the corresponding equilibrium system, the hard-rod fluid. Langevin dynamics simulations show that the motor activity enhances the tendency for nematic ordering. We develop a quantitative theory for the location of the phase boundary as a function of motor density. At high detachment forces of motors, we also observe filament clusters arising from blocking effects.

DOI: 10.1103/PhysRevLett.96.258103 PACS numbers: 87.16.Ka, 82.35.Gh, 87.16.Uv

Introduction.—In biological cells, small forces generated by motor proteins organize and rearrange cytoskeletal filaments and give rise to active, nonequilibrium filament dynamics, which plays an important role for cell division, motility, and force generation [1]. Whereas conventional "passive" polymer dynamics is driven by thermal fluctuations [2], active filament dynamics is characterized by a constant supply of mechanical energy by motor proteins, which hydrolyze adenine triphosphate. Active filament dynamics has been studied *in vitro* using solutions of microtubules and two-headed kinesin motor proteins [3], where the formation of patterns such as asters and vortices is observed. Theoretical studies of such patterns [4–8] have used a coarse-grained continuum description with kinetic equations for filament density and orientation fields and a motor-density field. In these approaches it is inherently difficult to relate the macroscopic transport coefficients of such descriptions to the experimentally accessible microscopic parameters of the system. Based on experimental work on actin solutions containing myosin motor minifilaments [9] it has been suggested that the effect of motor activity can be described by an increased effective temperature in the nonequilibrium system [10].

In this Letter, we study dynamics and pattern formation of many filaments in motility assays, where filaments glide over a planar substrate driven by motor proteins whose tails are anchored to the substrate. Motility or gliding assays are by now a standard tool to characterize motor proteins by analyzing the transport velocities of *single* filaments. In this work, we focus on the *cooperative* behavior of many filaments, which are transported in a confined two-dimensional assay such that a hard-core repulsion is effective. This system has been considered previously only on a coarse-grained level using a mapping to a spin model [11]. The equilibrium system corresponding to the motility assay in the absence of motors is the two-dimensional hard-rod fluid, which exhibits an isotropic-nematic ordering transition [12,13]. In this Letter, we show both numerically and analytically that the nematic ordering is enhanced by the presence of motor activity due to the combined effect of hard-core filament interactions and active forces exerted by the motors; see Fig. 1. Using previous results for the persistent motion of single filaments [14–16], we extend the dynamic mean-field theory for nematic ordering [17] to active systems. From the theoretical treatment, we derive the concept of an increased effective length, which successfully explains our simulation data and allows one to obtain the phase behavior in terms of the experimentally accessible microscopic model parameters.

Model.—Our microscopic model for motility assays describes filament configurations, motor heads, and polymeric motor tails as separate degrees of freedom. One end of the motor tail is anchored to the substrate, and the motor head on the other end can bind to a filament in the correct orientation due to the tail flexibility. Once bound, the motor head moves along the filament thereby stretching the polymeric tail, which gives rise to a loading force acting both on the motor head and the attached filament. This force feeds back onto the motion of the bound motor head, which moves with a load-dependent motor velocity [18]. Filaments follow an overdamped dynamics with external

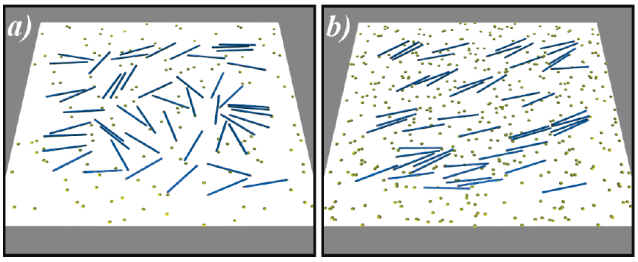

FIG. 1 (color). Snapshots of rodlike filaments on a motor coated substrate with randomly distributed motors and periodic boundary conditions. The filament concentration is $\rho = 2/L^2$, i.e., below the critical concentration of the equilibrium isotropic-nematic transition. For detachment forces $F_d = F_{\mathrm{st}}$, we find (a) an isotropic phase at low motor surface density $\sigma \ell_m L = 0.03$ and (b) active nematic ordering at high motor surface density $\sigma \ell_m L = 0.09$.

forces from the stretched motor tails and the repulsive filament-filament interaction [19].

To proceed, let us consider N rigid filaments of length L (with index $i = 1, \ldots, N$) on a planar substrate. The configuration of filament i can then be specified by the two-dimensional vector $\mathbf{r}_i$ for its center of mass and by the angle θ_i or the unit vector $\mathbf{u}_i = (\cos\theta_i, \sin\theta_i)$ for its orientation; see Fig. 2. The filament is subject to forces $\mathbf{F}_i^\alpha$ from N_i attached motors (with index $\alpha = 1, \ldots, N_i$) with motor heads positioned at $\mathbf{r}_i^\alpha$. Each such force arises from the polymeric tail of motor α, which is stretched by the directed motion of the motor head on the filament, which will be described below. We model the polymeric tail as a freely jointed chain such that $\mathbf{F}_i^\alpha$ is obtained by inverting the force-extension relation of a freely jointed chain [20]. In addition to motor forces, there are purely repulsive interaction forces $\mathbf{F}_{ij}$ from the hard-rod interaction between two filaments i and j of diameter D.

Under the influence of the motor forces $\mathbf{F}_i^\alpha$ and the interaction forces $\mathbf{F}_{ij}$ each filament i performs an overdamped translational motion, which is described by the stochastic Langevin-type equation of motion

$$\mathbf{\Gamma} \cdot \partial_t \mathbf{r}_i = \sum_{\alpha=1}^{N_i} \mathbf{F}_i^\alpha + \sum_{j=1}^{N} \mathbf{F}_{ij} + \boldsymbol{\zeta}_i, \qquad (1)$$

where $\mathbf{\Gamma}$ is the matrix of translational friction coefficients, which is given by friction coefficients $\Gamma_\parallel$ and $\Gamma_\perp$ for motion parallel and perpendicular to the filament orientation $\mathbf{u}_i$, respectively, and $\boldsymbol{\zeta}_i(t)$ are the Gaussian distributed thermal random forces [22].

In addition to filament translation, motor and interaction forces give also rise to the torques $M_i^\alpha = |(\mathbf{r}_i^\alpha - \mathbf{r}_i) \times \mathbf{F}_i^\alpha|$ and M_{ij}, respectively. These torques lead to an overdamped rotational dynamics, which is described by $\Gamma_\theta \partial_t \theta_i = \sum_{\alpha=1}^{N_i} M_i^\alpha + \sum_{j=1}^{N} M_{ij} + \zeta_{\theta,i}$, where Γ_θ is the rotational friction coefficient and $\zeta_{\theta,i}(t)$ is a Gaussian distributed thermal random torque [22]. Note that all friction coefficients $\Gamma_\parallel$, $\Gamma_\perp$, and Γ_θ are known from the passive filament dynamics.

The dynamics of motor heads is described by a deterministic equation of motion $\partial_t x_i^\alpha = v(\mathbf{F}_i^\alpha)$, where $|x_i^\alpha| \leq L/2$ defines the position of the motor α along the rod i, i.e., $\mathbf{r}_i^\alpha = \mathbf{r}_i + x_i^\alpha \mathbf{u}_i$, and the filament polarity is such that the motor head moves in the direction $\mathbf{u}_i$. The motor velocity v is a function of the loading force $\mathbf{F}_i^\alpha$ which builds up due to stretching of the motor tail. We use a force-velocity relation with a maximum value $v_{\max}$ for forces $\mathbf{F}_i^\alpha \cdot \mathbf{u}_i \geq 0$ pulling the motor forward, a linear decrease for forces $\mathbf{F}_i^\alpha \cdot \mathbf{u}_i < 0$ pulling the motor backwards, and $v = 0$ for $\mathbf{F}_i^\alpha \cdot \mathbf{u}_i < -F_{\text{st}}$, where F_{st} is the stall force [18].

We assume that the motor binds to the filament when the distance between the anchored end of the motor tail at $\mathbf{r}_0^\alpha$ and the filament is smaller than a capture radius ℓ_m. Apart from the stall force F_{st} the motor is also characterized by its detachment force F_d, above which the unbinding rate of the motor head becomes large. For simplicity we assume in our model that the motor head detaches whenever the force F_i^α exceeds a threshold value F_d. We consider the case of processive motors with a high duty ratio close to unity; i.e., motors detach from a filament only if they reach the filament end or if the total force becomes larger than the detachment force F_d.

Simulation.—Using the above model we performed simulations of gliding assays for a random distribution of motors with a surface density σ and periodic boundary conditions. At each time step Δt, we update the motor head positions x_i^α and filament positions and orientations using the discretized versions of the equations of motions described above. The parameter values that we choose for the simulations are comparable with experimental data on assays for conventional kinesin. The simulation results presented in Figs. 1 and 3 have been obtained for quadratic assays of area 25 μm^2 with filaments of length $L = 1$ μm and diameter $D = L/40$ at room temperature $T \simeq 4 \times 10^{-3}$ pN μm. Friction coefficients are $\Gamma_\perp = 2\Gamma_\parallel = 4\pi\eta L/\ln(L/D)$ and $\Gamma_\theta = \Gamma_\parallel L^2/6$, where η is the viscosity of the surrounding liquid. We use a value $\eta = 0.5$ pN s/μm^2 much higher than the viscosity of water, $\eta_{\text{water}} \sim 10^{-3}$ pN s/μm^2, which allows one to take larger simulation time steps. We checked that this does not affect results. We use a maximum motor speed of $v_{\max} = 1$ $\mu\text{m s}^{-1}$ and a stall force of $F_{\text{st}} = 5$ pN. The capture radius for motor proteins is $\ell_m = 10^{-2}$ μm and the length of the fully stretched motor tail is $L_m = 5 \times 10^{-2}$ μm.

Phase behavior.—Motor activity strongly modifies the nematic ordering of rigid filaments of length L in a motility assay. Therefore, both the rod density ρ and the motor density σ are essential in order to determine the phase behavior, which can be described in the plane of the two dimensionless parameters ρL^2 and $\sigma \ell_m L$. Nematic ordering in a system of N filaments can be characterized by the time averages of the order parameter $S \equiv \sum_{i \neq j} \cos[2(\theta_i - \theta_j)]/N(N-1)$ with $\langle S \rangle = 0$ in the isotropic phase and $\langle S \rangle = 1$ for perfect nematic order. In equilibrium, i.e., in the absence of motors ($\sigma = 0$), we find a continuous isotropic-nematic transition at a critical density $\rho_{c,0} \simeq 4.3/L^2$ in the simulation, which is in good agreement with the analytic result $\rho_c = 3\pi/2L^2$ based on Onsager's

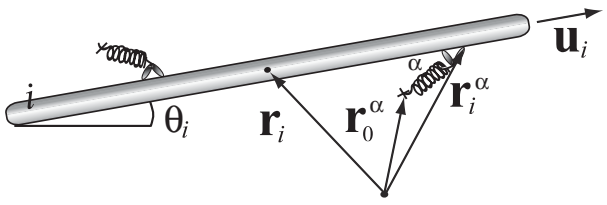

FIG. 2. Schematic top view of a filament i in the motility assay with two motors attached. $\mathbf{r}_i$ is the filament's center of mass, and θ_i and $\mathbf{u}_i$ its orientational angle and unit vector, respectively. The attached motor α is anchored at $\mathbf{r}_0^\alpha$, and its head is positioned at $\mathbf{r}_i^\alpha$.

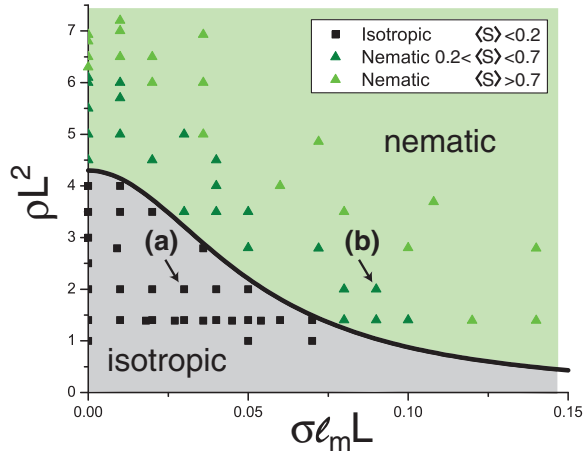

FIG. 3 (color). The phase diagram of the gliding assay as a function of the dimensionless filament density ρL^2 and the dimensionless surface motor density $\sigma \ell_m L$ for a detachment force $F_d = F_{\rm st}$ and $L/\ell_m = 100$. All data points correspond to separate simulation runs, the two arrows (a) and (b) to the snapshots in Fig. 1. If the average order parameter $\langle S\rangle < 0.2$, the system is in the isotropic phase (black squares, gray area), if $\langle S\rangle > 0.2$ it is in the nematic phase (green triangles, green area). The solid line represents the analytical result (5).

theory [13]. The equilibrium transition is found numerically from the inversion point of the curve $\langle S\rangle = \langle S\rangle(\rho)$ for a value $\langle S\rangle \simeq 0.2$, which we also use as the threshold value for active nematic ordering if motors are present ($\sigma > 0$); see Fig. 3. Snapshots of the actively driven system in the isotropic and nematic phase are shown in Figs. 1(a) and 1(b), respectively. In the resulting phase diagram (Fig. 3), the critical density ρ_c for active nematic ordering *decreases* with increasing motor density; i.e., nematic ordering is favored if more energy is fed into the system. The transition is continuous also for nonzero motor density; see the order parameter plots in [19]. Note that in the presence of motor activity, there is a nonvanishing filament current in the nematic phase, which is characteristic for a nonequilibrium phase.

Mutual blocking of filaments can lead to kinetically arrested filament clusters as shown in Fig. 4. We find that stable clusters appear if the detachment force F_d is large compared to the stall force $F_{\rm st}$ such that the maximal force transmitted to a filament through collisions does not lead to detachment of the filament and dissolution of the cluster. Because collisions between filaments are exceptional in the isotropic phase, clusters occur primarily in the nematic phase region.

The motion of a filament is characterized by stochastic switching between rotational and translational diffusion if no motors are attached, directed translation in rotationally diffusing directions if one motor is attached, and directed translation if two or more motors are attached. The relative frequency of these types of motion depends on the mean distance $\langle d_m\rangle$ between bound motors and, thus, on the surface motor concentration σ [14]. For high motor concentrations a filament has two or more bound motors on average and $\langle d_m\rangle \sim 1/\sigma\ell_m$. The single filament performs a persistent walk with a persistence length [14]

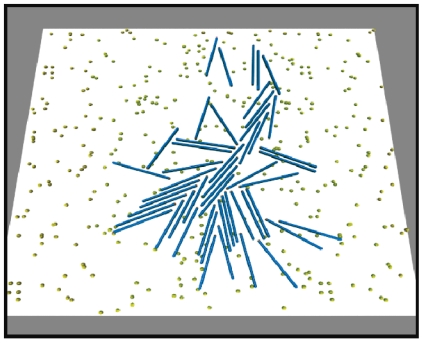

FIG. 4 (color). Snapshot of a cluster of mutually blocking filaments for large detachment force $F_d = 10F_{\rm st}$ using otherwise the same parameters as in Fig. 1(b) [$\rho = 2/L^2$, $\sigma\ell_m L = 0.09$].

$$\xi_p = \frac{L + 2\langle d_m\rangle}{L + 3\langle d_m\rangle}\frac{L^3}{9\ell_m^2}\left(e^{L/\langle d_m\rangle} - 1 - \frac{L}{\langle d_m\rangle}\right) \qquad (2)$$

corresponding to a persistence time $t_p = \xi_p/v_F$, where v_F is the mean filament velocity. This velocity can be obtained by simultaneously equating (i) the filament friction force with the total motor driving force and (ii) the filament velocity with the motor velocity in the steady state, which gives $v_F = v_{\rm max}(1 + \Gamma_\parallel v_{\rm max}\langle d_m\rangle/LF_{\rm st})^{-1}$. A coarse graining in time by averaging over time intervals of one persistence time t_p leads to an effective random walk of a single filament. On time scales larger than t_p the dynamics of a filament is again described by a diffusion equation as for passive dynamics. In the mean-field approximation the average number density of rodlike filaments $f(\mathbf{r}, \mathbf{u}, t)$ in the configuration $(\mathbf{r}, \mathbf{u})$ satisfies the following Smoluchowski equation [2,17]:

$$\begin{aligned}\partial_t f = {} & T\boldsymbol{\nabla}_\mathbf{r}\cdot\boldsymbol{\Gamma}^{-1}\cdot(\boldsymbol{\nabla}_\mathbf{r} f + f\boldsymbol{\nabla}_\mathbf{r}\bar{W}) \\ & + T\Gamma_\theta^{-1}\mathcal{R}_\mathbf{u}[\mathcal{R}_\mathbf{u} f + f\mathcal{R}_\mathbf{u}\bar{W}],\end{aligned} \qquad (3)$$

where $\mathcal{R}_\mathbf{u} \equiv \mathbf{u}\times\partial_\mathbf{u}$ is the rotational operator. Translational and rotational diffusion operators decouple after coarse graining to one persistence time. $T\bar{W} \equiv \int d\mathbf{r}' d\mathbf{u}' W(\mathbf{r}-\mathbf{r}', \mathbf{u}, \mathbf{u}') f(\mathbf{r}', \mathbf{u}', t)$ is a steric mean-field interaction, while $TW(\mathbf{r}-\mathbf{r}', \mathbf{u}, \mathbf{u}')$ represents the steric interaction potential between two filaments with center of masses and orientations $(\mathbf{r}, \mathbf{u})$ and $(\mathbf{r}', \mathbf{u}')$. The directed motion due to motors increases the interaction range of filaments. During a persistence time t_p two filaments in configurations $(\mathbf{r}, \mathbf{u})$ and $(\mathbf{r}', \mathbf{u}')$ collide if the connection vector $\mathbf{r} - \mathbf{r}'$ can be constructed as a linear combination $\mathbf{u}\xi + \mathbf{u}'\eta$ with $-L/2 < \xi, \eta < L/2 + \xi_p$, and $|\xi - \eta| < L/2$. Therefore, we obtain a steric interaction potential

$$\begin{aligned}W = {} & |\mathbf{u}\times\mathbf{u}'| \iint_{-L/2}^{L/2+\xi_p} d\xi d\eta \Theta_L(\xi-\eta) \\ & \times \delta(\mathbf{r} - \mathbf{r}' + \mathbf{u}\xi + \mathbf{u}'\eta),\end{aligned} \qquad (4)$$

where $\Theta_L(\xi - \eta)$ equals one if $|\xi - \eta| < L/2$ and zero otherwise. Performing an analogous stability analysis as in Ref. [17] using the modified interaction potential (4), we finally obtain the critical filament density of the active isotropic-nematic transition,

$$\rho_c = c/L[L + \xi_p(\langle d_m \rangle, \ell_m, L)], \quad (5)$$

with $c = 3\pi/2$ from the analytical mean-field calculation [23]. In the absence of motors we have $\xi_p = 0$ and the result (5) reduces to the equilibrium result of Ref. [13]. Using the result (2) for the persistence length ξ_p we obtain an explicit expression of the isotropic-nematic phase boundary in terms of the microscopic model parameters, which is in good agreement with all simulation data; see Fig. 3. Beyond mean field, we expect a larger prefactor c in (5) but the same parameter dependence.

The result (5) corresponds to an *effectively increased filament length* $L_{\text{eff}} = \sqrt{L(L + \xi_p)}$ as compared to the equilibrium system, which explains that motor activity actually favors nematic ordering. In deriving (4), we have established a mapping of the nonequilibrium driven system onto an equilibrium system with larger effective filament length. This mapping applies only within the isotropic phase as it is based on the statistical properties of the motion of a single filament but can be used to calculate the stability boundary (5) of the isotropic phase. The motor activity also increases the effective diffusion constant of single filaments to $D_{\text{eff}} \sim D + \xi_p v_F$ [14–16]. Thus, using the Einstein relation $D = T(\Gamma_\parallel^{-1} + 2\Gamma_\perp^{-1})/3$ [2] we might define an increased effective temperature $T_{\text{eff}} \sim T + 3\xi_p v_F/(\Gamma_\parallel^{-1} + 2\Gamma_\perp^{-1})$ for the isotropic phase. For steric filament interactions, however, this effective temperature does *not* influence the phase behavior.

Experimental realization.—Confinement of filaments to strictly two dimensions is hard to realize experimentally but it has been observed that microtubules in a dynein motility assay exhibit hard-core interactions also in the absence of such a confinement [24]. Alternatively, we propose to consider a three-dimensional filament solution that is confined between two plates with anchored motors. The motor activity can induce an active *surface* nematic ordering of the filaments, which eventually propagates into the bulk if the filament density is sufficiently close to the critical density of the equilibrium Onsager transition in three dimensions.

Conclusion.—We have presented simulations and a theoretical description of the phase behavior of filaments in a two-dimensional motility assay. The corresponding equilibrium system is the two-dimensional hard-rod fluid, which exhibits an isotropic-nematic phase transition. We have found that actively driven systems undergo an analogous phase transition and the motor activity *enhances* the tendency for nematic ordering. A similar enhancement is found in three-dimensional active filament solutions [5]. For the two-dimensional motility assays we have quantitatively determined the phase boundary (5) for active nematic ordering by motors in terms of experimentally accessible microscopic model parameters. For high motor detachment forces $F_d \gg F_{\text{st}}$, we also find kinetically arrested filament clusters within the nematic phase region.

This work was supported by the EC Sixth Framework Program (as part of the STREP Active Biomics Contract No. NMP4-CT-2004-516989).

[1] J. Howard, *Mechanics of Motor Proteins and the Cytoskeleton* (Sinauer Associates, Inc., Sunderland, 2001).
[2] M. Doi and S. F. Edwards, *The Theory of Polymer Dynamics* (Clarendon, Oxford, 1986).
[3] F. J. Nédélec *et al.*, Nature (London) **389**, 305 (1997); T. Surrey *et al.*, Proc. Natl. Acad. Sci. U.S.A. **95**, 4293 (1998); **95**, 4293 (1998).
[4] H. Y. Lee and M. Kardar, Phys. Rev. E **64**, 056113 (2001).
[5] T. B. Liverpool and M. C. Marchetti, Phys. Rev. Lett. **90**, 138102 (2003).
[6] K. Kruse *et al.*, Phys. Rev. Lett. **92**, 078101 (2004).
[7] I. S. Aranson and L. S. Tsimring, Phys. Rev. E **71**, 050901(R) (2005).
[8] F. Ziebert and W. Zimmermann, Phys. Rev. E **70**, 022902 (2004).
[9] D. Humphrey *et al.*, Nature (London) **416**, 413 (2002).
[10] T. B. Liverpool *et al.*, Phys. Rev. Lett. **86**, 4171 (2001).
[11] B. Bassetti *et al.*, Eur. Phys. J. B **15**, 483 (2000).
[12] L. Onsager, Ann. N.Y. Acad. Sci. **51**, 627 (1949).
[13] R. F. Kayser and H. J. Raveché, Phys. Rev. A **17**, 2067 (1978).
[14] T. Duke *et al.*, Phys. Rev. Lett. **74**, 330 (1995).
[15] M. R. Faretta and B. Basetti, Europhys. Lett. **41**, 689 (1998).
[16] F. Gibbons *et al.*, Biophys. J. **80**, 2515 (2001).
[17] M. Doi, T. Shimada, and K. Okano, J. Chem. Phys. **88**, 4070 (1988); T. Shimada, M. Doi, and K. Okano, J. Chem. Phys. **88**, 7181 (1988).
[18] C. M. Coppin *et al.*, Proc. Natl. Acad. Sci. U.S.A. **94**, 8539 (1997); S. M. Block *et al.*, *ibid.* **100**, 2351 (2003).
[19] See EPAPS Document No. E-PRLTAO-97-024627 for an appendix containing a detailed description of our model. For more information on EPAPS, see http://www.aip.org/pubservs/epaps.html.
[20] If the motor tail is anchored at $\mathbf{r}_0^\alpha$, the force $-\mathbf{F}_i^\alpha$ is pointing in the directions $\Delta\mathbf{r}^\alpha \equiv \mathbf{r}_i^\alpha - \mathbf{r}_0^\alpha$ and $|\Delta\mathbf{r}^\alpha|/L_m = f_{\text{FJC}}(|\mathbf{F}_i^\alpha| b_m/T)$, where L_m is the contour and b_m the monomer length of the polymeric motor tail, and $f_{\text{FJC}}(x) \equiv 1/\tanh x - 1/x$; cf. [21].
[21] J. Kierfeld *et al.*, Eur. Phys. J. E **14**, 17 (2004).
[22] $\mathbf{\Gamma} = \Gamma_\parallel \mathbf{u}_i \otimes \mathbf{u}_i + \Gamma_\perp(\mathbf{I} - \mathbf{u}_i \otimes \mathbf{u}_i)$ [2], where $\mathbf{I}$ is the unit matrix and $\otimes$ the dyadic vector product. Thermal noise $\boldsymbol{\zeta}_i(t)$ and thermal torque $\zeta_{\theta,i}(t)$ have correlations $\langle \boldsymbol{\zeta}_i(t) \otimes \boldsymbol{\zeta}_j(t') \rangle = 2T\mathbf{\Gamma}\delta_{ij}\delta(t - t')$ and $\langle \zeta_{\theta,i}(t)\zeta_{\theta,j}(t') \rangle = 2T\Gamma_\theta \delta_{ij}\delta(t - t')$.
[23] In three dimensions the corresponding result is $\rho_c^{3d} = c^{3d}/DL[L + \xi_p^{3d}]$, with $\xi_p^{3d} = \xi_p \pi^2 L^2/4\ell_m^2$ and $c^{3d} = 4\pi/3$.
[24] Kazuhiro Oiwa (private communication).